High-speed laser absorption measurements of carbon oxides in linear detonation channels

Kyle L. Fetter*, Benjamin R. Steavenson*, Brandon M. Ng*, Angelina Andrade*, Christopher S. Combs[†], Daniel I. Pineda[‡] The University of Texas at San Antonio, San Antonio, TX, 78249

John W. Bennewitz§

The University of Alabama in Huntsville, Mechanical and Aerospace Engineering Department, Huntsville, AL 35899

Jason R. Burr[¶]

AFRL/RQRC, Combustion Devices Branch, U.S. Air Force Research Laboratory, Edwards Air Force Base, CA 93524

Blaine R. Bigler Jacobs Technology, Inc., Edwards Air Force Base, CA 93524

A mid-infrared laser absorption sensing strategy for carbon monoxide (CO) and carbon dioxide (CO₂) has been deployed for application to detonation flows in a linear channel with dimensions relevant to RDRE investigations at the U.S. Air Force Research Laboratory (AFRL) at Edwards Air Force Base. Bias-tee circuitry integrated with a distributed feedback quantum cascade laser near 4.94 μ m and an interband cascade laser near 4.19 μ m has enabled MHz-rate wavelength scanning, capturing a cluster of P-branch transitions of CO and a cluster of R-branch transitions of CO₂. The mid-infrared light sources were both aligned onto a single detector in a compact optical arrangement, and diplexed in time to reduce the integration time of the measurements to 500 ns while maintaining sufficient wavelength scan depth to resolve the features of interest. Post-detonation CO mole fraction values were inferred from a multi-line spectral fitting routine and CO₂ mole fraction values were inferred using a collisional line mixing model developed previously. Quantitative mole fraction measurements were obtained behind gaseous methane/oxygen detonation waves in a linear, optically-accessible detonation channel at AFRL, reflective of rotating detonation engine geometries relevant to detonation propulsion research projects at AFRL.

I. Introduction

Detonation-based combustion has received considerable interest for rocket propulsion applications over the last several years, owing to several potential advantages in practical design [1] and theoretical efficiency gains [2]. Recent advances in high-speed laser absorption diagnostics [3] have enabled quantitative assessment of temperature, pressure, and species mole fraction in rotating detonation combustors, motivating rigorous analysis of gas phase thermodynamics in these devices. Through rigorous testing under advanced diagnostics and instrumentation, possible reasons for RDRE performance shortcomings have been suggested, including propellant mixedness [4], injector dynamics [5], and parasitic deflagration [6]. Although convenient for investigations at higher Technology Readiness Levels (TRLs), the RDRE architecture convolutes multiple physics simultaneously, and the extensive heat transfer present in many current experimental configurations influences the system energy balance [7].

To reduce the experimental complexity and enable more fundamental but still-relevant RDRE investigations, a linear detonation channel facility has recently been developed at the Air Force Research Laboratory (AFRL) at Edwards Air Force Base, providing a test bed for various optical diagnostics and advanced instrumentation to interrogate the detonation

^{*}Graduate Research Assistant, Department of Mechanical Engineering, AIAA Student Member

[†]Assistant Professor, Department of Mechanical Engineering, AIAA Senior Member

[‡]Assistant Professor, Department of Mechanical Engineering, AIAA Member

[§] Assistant Professor, Department of Mechanical and Aerospace Engineering, AIAA Senior Member

Research Scientist, AFRL/RQRC, 10 East Saturn Blvd., Edwards AFB, CA, 93524. AIAA Member

Research Scientist, Jacobs Technology, Inc., 10 East Saturn Blvd., Edwards AFB, CA, 93524. AIAA Member

of multiple fuels under highly-controlled conditions. In this paper, we describe the testing and preliminary assessment of a scanned-wavelength laser absorption-based sensing strategy to perform quantitative high-speed, time-resolved measurements of species concentration (i.e., X_{CO} , X_{CO_2}) behind detonation waves fueled by gaseous propellants in the AFRL facility.

II. Laser Absorption Spectroscopy Theory and Background

The theory of laser absorption spectroscopy (LAS) is well-documented [S], and briefly discussed here to clarify notation. The Beer-Lambert law in Eqn. Telates the spectrally-resolved absorbance of rovibrational transition i to thermochemical gas properties, including pressure P [atm], temperature T [K], and absorbing species mole fraction X in a uniform gas of pathlength L [cm] at a wavenumber v [cm $^{-1}$]:

$$\alpha_{\nu} = -\ln\left(\frac{I_t}{I_0}\right)_{\nu} = PXS_i(T)\varphi_i(\nu)L \tag{1}$$

where $S_i(T)$ is the temperature-dependent linestrength and $\varphi(v)$ is the lineshape function.

For all experiments described in this study, a scanned-wavelength direct absorption technique is utilized to scan across the wavelength domain of the target rovibrational transitions. Once the absorbance of the targeted transitions are collected, the features are spectrally-fitted to infer mole fraction. For CO, we target the P(1,22) and the P(3,10) transitions near 2025 cm⁻¹, and implement a nonlinear least-squares fitting routine $\boxed{9}$ assuming a Voigt lineshape model, wherein temperature and mole fractions estimated from Chapman-Jouguet (CJ) detonation models $\boxed{10}$ were used to initially simulate and subtract absorbance associated with interfering water vapor (H₂O) spectra. Collisional broadening was modeled for each collisional partner of each target transition, as described by Eqns. $\boxed{2}$ and $\boxed{3}$. The collisional width, Δv_C , is calculated based on pressure P, molar concentration of the collisional partner X_A , and the broadening coefficient of the partner γ_{B-A} , which is a function of temperature T and the coefficients specific to each transition, $\gamma(T_0)$ and N. Broadening partners were obtained from the HITEMP database $\boxed{11}$ and the literature $\boxed{12}$.

$$\Delta v_C = P \sum X_A 2 \gamma_{B-A} \tag{2}$$

$$2\gamma_{B-A} = 2\gamma(T_0) \left(\frac{T_0}{T}\right)^N \tag{3}$$

For CO_2 , we leverage the high differential absorbance caused by the phenomenon of *line mixing* [13] in the bandhead of the v_3 ($0 \rightarrow 1$) fundamental band near 2385 cm⁻¹. This phenomena counteracts the detrimental effects of collisional broadening on differential absorption, enabling more robust high-pressure and -temperature measurements of CO_2 . However, owing to this phenomenon, spectral fitting assuming simple summation of line-by-line absorbance—as is performed for CO in this study—is insufficient to interpret the spectra. The collisional broadening and the interactions between the transitions are modeled using the collisional line mixing model and the relaxation matrix shown in Eqns. [4]. The absorbance of the bandhead feature described by Eqn. [4] is described by the number density of the gas N, the pathlength L, and the imaginary components the dipole of all the bandhead transitions \mathbf{d} , the inverse of the matrix combining the wavelength range v, the transition linecenters of all the bandhead transitions v_0 , pressure, and the relaxation matrix \mathbf{W} , and finally the diagonal matrix comprising the difference of the energy states for each transition ρ .

$$\alpha_{\nu} = \frac{NL}{\pi} Im \left(\mathbf{d} * (\nu \mathbf{I} - \nu_0 - iP \mathbf{W}_{\mathbf{J}\mathbf{K}})^{-1} * \rho * \mathbf{d} \right)$$
 (4)

The relaxation matrix **W** component parts are described in Eqn. 5. The diagonal components correspond to the broadening effects of each line with the deviation for the linecenter. The off diagonal components correspond to the Modified Energy Gap fitting law (MEG) $(R_J^{"} \leftarrow K^{"})$ and the temperature dependence of the fit (A_{RR}) .

$$W_{JK} = \begin{cases} \gamma_J - i\Delta \nu_{0J} & \text{if } J = K \\ -A_{RR} R_{J^" \longleftarrow K^"} & \text{if } J \neq K \end{cases}$$
 (5)

More detail on the theory and application of spectral line mixing models for CO_2 to rocket propulsion flows can be found in the works of Lee et al. [14, [15]].

Sensing in high temperature and pressure environments—such as those observed in detonations—has been notoriously difficult due to increased collisional broadening at high pressures [16]. Further challenging the issue, limitations in

laser controller bandwidth—compounded with historically low scan depths of mid-infrared light sources relative to those in the near-infrared—have long inhibited high-time resolution measurements via scanned-wavelength methods. However, recent advancements in both high-speed wavelength-scanning methods [17] and high-pressure measurement strategies [18] [19] have enabled quantitative measurements in high-pressure detonation waves. In the following section we describe our approach to leverage these recent technology advances to perform such measurements.

III. Experimental Setup and Optical Diagnostic Methodology

Experiments were performed on a linear detonation channel developed at AFRL-Edwards, with a rectangular cross section of 50 mm x 5 mm and an overall length of 2 m. Detonable mixtures are ignited outside of the linear channel facility with a spark plug contained in a brass mixing manifold, which is connected by stainless steel tubing to a branched initiator inside the channel facility, appearing in the leftmost channel section in Fig. [I]. Inert gases and propellants are supplied to the linear detonation channel though a mixing manifold connected to multiple propellant supply lines, with flow rates of the gaseous propellants controlled by critical flow venturi nozzles (CFVNs) and solenoid valves, and recorded by pressure transducers on both sides of the CFVNs. A diagram of the propellant handling infrastructure, with key sections of the facility indicated, is shown in the bottom of Fig. [I].

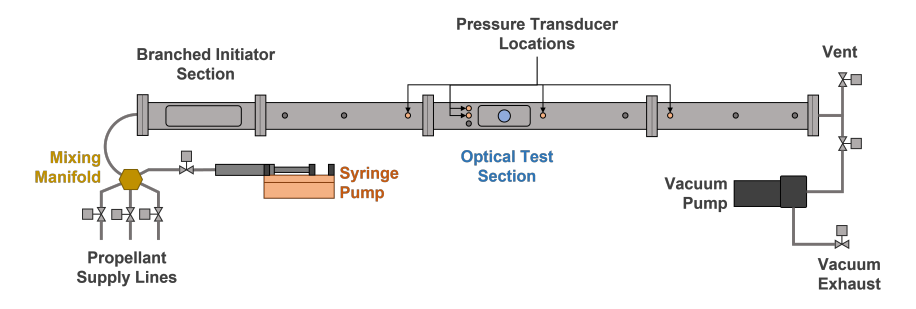


Fig. 1 Simplified Piping and Instrumentation Diagram for the Detonation Channel Facility at Edwards Air Force Base, with relevant plumbing infrastructure and mixture handling components shown.

The branched initiator section serves to successively multiply the initial nascent detonation wave into multiple small channels (O(0.5 cm)) prior to entering the main channel (O(5 cm)). Upon exiting the branched initiator section, the detonation waves combine and coalesce into a single planar detonation wave which proceeds to travel through the rest of the linear detonation channel. The detonation channel sections are equipped with ports for the installation of dynamic pressure transducers. Transducer locations in the detonation channel used in this work are indicated by orange dots in of Fig. \blacksquare with unused ports shown in dark grey. A series of detonations were conducted using gaseous methane (CH₄) and gaseous oxygen (O₂) at varying equivalence ratios. Throughout the campaign, pressure data and LAS data were captured for individual test conditions comprising equivalence ratios $\phi = 0.6, 0.8, 1.0, 1.2, 1.4$, and 1.6.

For LAS measurements to be conducted on the detonation channel at AFRL, specific modifications were necessary to enable optical access for the chosen wavelengths to probe CO and CO₂. Specifically, a mid-infrared-transparent material, such as sapphire, was required for optical access through the detonation channel. As part of this study, an optical view port arrangement which used commercial off-the-shelf sapphire windows was designed for installation in the detonation tunnel facility to enable mid-wave infrared transmission. The window was completed and installed into the channel with no observed issue prior to or during operation.

A continuous-wave distributed feedback (DFB) interband cascade laser (ICL) and quantum cascade laser (QCL) tunable from 2381 cm⁻¹ to 2387 cm⁻¹ and 2018 cm⁻¹ to 2028 cm⁻¹ respectively were modulated using bias-tee circuitry [3] [17] to target CO₂ and CO, respectively. For the optical setup at AFRL shown in Fig. [2], both laser beams were pitched co-linearly through an optically-accessible detonation channel and collected using a single high speed photovoltaic detector (VIGO PVMI-4TE-6-1x1). To diplex the beams of the two lasers onto a single detector, the injection-current function generation signals were duty-cycle modulated and offset from one another such that neither light source was lasing simultaneously into the detector. A 2-inch germanium etalon fixed to an optical flip-mount was placed in the optical line-of-sight before each experiment to determine the relative wavenumber of the laser light during the scan [3].

Generally, laser scan depth decreases as scan rate increases for distributed feedback quantum and interband cascade

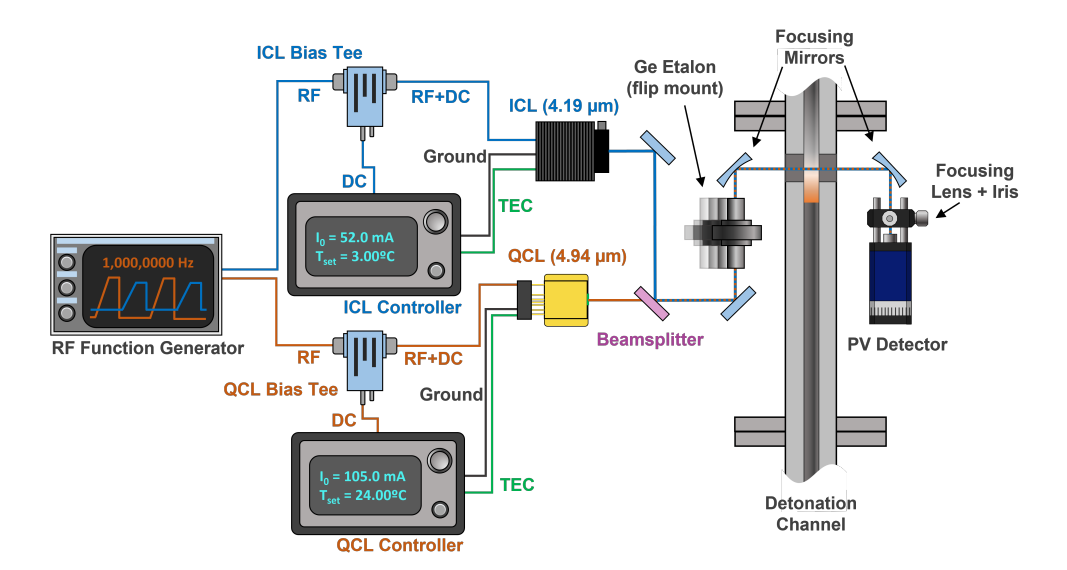


Fig. 2 Simplified optical setup diagram for the sensing strategy used in this work, with optoelectronic connections highlighted.

lasers [3] [7]. We overcome this limitation by implementing the aforementioned bias-tee circuitry and the use of extended square-wave injection-current scans, which have been shown to dramatically increase scan depth at high scan frequencies. To optimize the increased scan-depth at these MHz scan rates, multiple injection-current scanning techniques and waveforms were investigated, including "threshold-bound sine" and "extended square" waveforms with multiple duty cycles, as described by Nair et al. [17]. We observed that for both the ICL and QCL, implementation of the bias-tee circuitry increases the scan depth at higher scan rates, with the extended square wave type allowing for the greatest scan depth among the techniques investigated. The greatest boost in scan depth was observed for the QCL, which has a much higher lasing threshold current (~90 mA) than that of the ICL (~30 mA).

IV. Results and Discussion

All measurements reported in this study on the linear detonation channel facility at AFRL involved the extended square waveform technique enabled by the bias-tee circuitry, and all tests were conducted at a laser scan rate of 1 MHz. We observed that typical scan depths at this frequency for the ICL and QCL were 0.35 and 0.6 cm⁻¹ respectively. The spectral models employed in this study to interpret the absorbance over those wavelength ranges were initially validated against both simulated spectra (for the Voigt lineshape model used to interpret absorbance by CO) and previously collected [14, 15] experimental shock tube data (for the collisional line mixing model used to interpret absorbance by CO₂). Once the spectral models were validated, they were incorporated into fitting routines using non-linear regression methods with absorbing species mole fraction, absolute wavenumber offset, and and a broadening multiplier for all relevant Δv_c as free parameters. Collisional broadening associated with the high pressures observed in the experiments (>20 atm) blended the spectral features too significantly to reliably perform two-line thermometry in either targeted wavelength region. Thus, pressure and temperature were treated as fixed parameters in the spectral fitting, assuming values from measured pressure transducer data and inferred temperature values from the Taylor expansion waves following the detonations, respectively. Residuals for the fits are generally below 10%, justifying application of the chosen spectral models to the experimental data collected behind the detonation waves. Owing to the relatively low differential absorption observed in the data collected for CO and sensitivity to assumed H₂O concentration, the fitted parameter uncertainties for CO mole fraction are much higher than those of CO₂. High differential absorption observed in the data collected for CO₂—primarily caused by collisional line mixing—reduced the fitted parameter uncertainties for CO₂ mole fraction. More detail on uncertainty estimates is provided in Section V.

Calculated CO and CO₂ concentrations behind CH₄/O₂ detonation waves are shown in Figs 3 and 4, alongside measured pressure and inferred temperature, plotted as a fraction of their theoretical CJ values, P_{CJ} and T_{CJ} , respectively. Calculated concentrations are plotted from the moment shortly ($\sim 1 \mu s$) after the detonation wave passes up until right

before the reflected shock wave from the detonation channel end-wall passes back through the LAS measurement region. For all tests, the peak pressure values in the detonation waves captured by the transducers were all lower than the calculated CJ pressure, P_{CJ} , by nearly 30%. There are several explanations for this observation, including that the pressure drop immediately after the CJ point occurs too rapidly for the pressure transducers to accurately resolve the max pressures of the waves as they are passing, or that transient heat losses to the walls reduced the overall strength of the detonation waves. Moreover, the chemical energy of the fuel may not be immediately released in one instant, as is assumed for the CJ detonation model, or the less-than-expected pressure gain encourages less-complete combustion than would have otherwise occurred. Although the preliminary relative uncertainty in reported CO mole fraction is fairly large (\sim 20%) and the CJ-predicted mole fraction does fall within those margins, this trend is persistent throughout all equivalence ratios tested, and a higher concentration of CO than expected is observed for some cases. The calculated temperatures (obtained with the pressure measurements assuming a Taylor expansion wave) shortly after (<10 μ s) the detonation wave passage and experimentally-obtained wave speeds of the detonation waves were determined to be within 10% of all theoretical CJ temperatures and wave speeds.

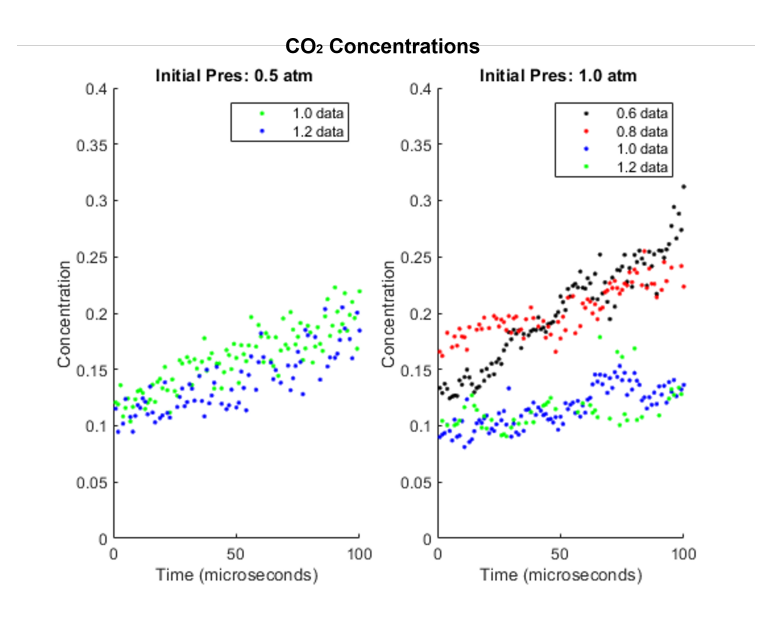


Fig. 3 Carbon Dioxide concentration comparison for CH₄/O₂ detonations (p_i = 1 atm, ϕ = 0.6, 0.8, 1.0, 1.2), (p_i = 0.5 atm, ϕ = 1.0, 1.2)

The CO_2 concentration measurements corresponding to the first $100 \,\mu s$ after the CH_4/O_2 detonation are shown in Fig. 3 Fig. 3 shows both the data for tests conducted two different initial pressures (0.5 atm, 1.0 atm). All concentrations for CO_2 trend higher in concentration over time, corresponding to decreases in both pressure reported by the pressure transducers and in temperature as calculated by the Taylor expansion wave assumption. As the concentration of CO_2 is not dropping (discussed for Fig. 4), this suggests that the concentration of CO_2 is unlikely to be increasing, and rather that the Taylor expansion wave assumption may not be appropriate for the time period significantly after the passage of the detonation wave. Further investigation with respect to the line mixing model of this $CO_2 \nu_3$ bandhead is warranted.

Carbon monoxide measurements corresponding to the first $100 \,\mu s$ after the CH_4/O_2 detonation are shown in Fig. 4. The concentrations after the detonation are observed to remain constant throughout the time frame. The NASA Chemical Equilibrium Analysis results for the Chapman-Jouguet condition concentrations were compared to the mean results of the measurements in the first $10 \,\mu s$ for all measured conditions. The results are shown in Fig. 5, showing CO_2 measurements for 0.5 and 1.0 atm, and CO measurements at 1 atm. Several simulated concentrations were observed within the measurement uncertainty; however, four conditions were observed with higher concentration compared to the predicted concentrations. Further investigation is needed to determine the source(s) of this inconsistency.

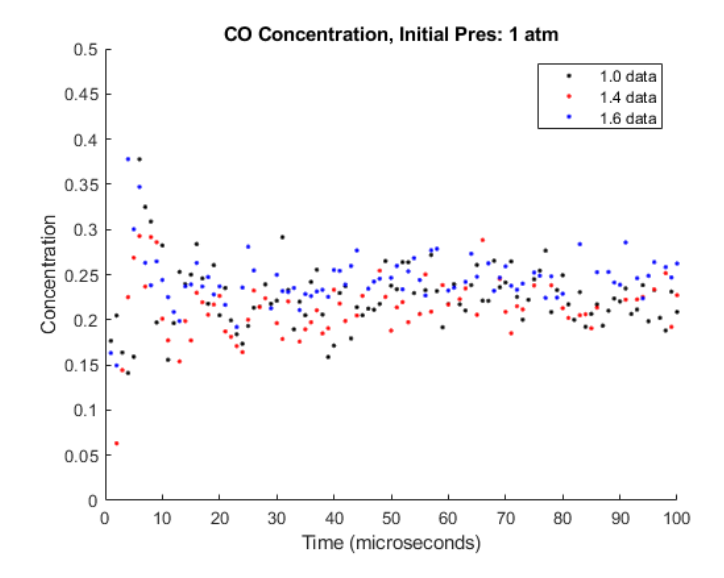


Fig. 4 Carbon monoxide concentration comparison for CH_4/O_2 detonations ($p_i = 1$ atm, $\phi = 1.0, 1.4, 1.6$)

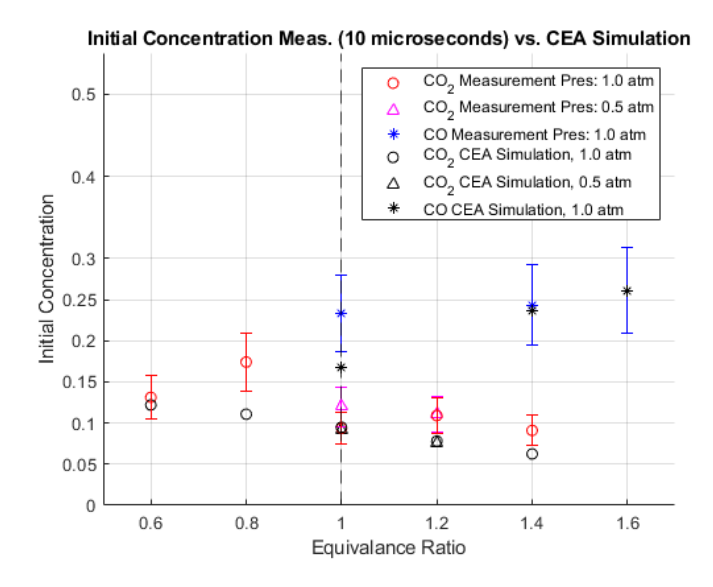


Fig. 5 All methane measurements compared to CEA concentration simulations

V. Uncertainty and Assumptions

The preliminary data reported here presently have higher-than-desirable experimental uncertainty, although it is anticipated that additional efforts to improve and refine the spectral models will reduce this uncertainty. It is important to note that to obtain quantitative results for the mole fraction of the carbon oxides that several assumptions were made regarding several parameters in both the experiment and the spectral models. We assumed that the concentration of the non-target post-detonation gases (e.g., all gases not CO and CO₂)—used to calculate collisional broadening effects—remained constant throughout the measurement period, and were assumed to be equal to the chemical equilibrium analysis (CEA) results. We also assume that H₂O remains in the gas phase during the time periods of the reported measurements.

A sensitivity analysis was performed on the models to determine the variation in the fitted parameters based on the uncertainty of the fixed parameters, e.g., input pressure, temperature, broadening parameters, collisional partner concentrations, and CJ CEA calculations. As many of these input parameters are coupled, we performed the sensitivity analysis by randomly distributing all uncertain values by their respective uncertainties and determining their effects on the outputs of both spectral models. All unknown uncertainties were assumed to have a standard deviation of 5% of the measured value, except for measured transducer pressure, which was given a conservative standard deviation of 10% based on the manufacturer's equipment data sheets. The spectral fitting routine for CO₂ had a relative uncertainty in output mole fraction (based on input parameter uncertainty) of 18% with 95% confidence, while that for CO had a relative uncertainty in output mole fraction of 23% with a 95% confidence.

VI. Summary and Future Work

In this study, high-speed LAS measurements of CO and CO₂ were examined following gaseous methane and oxygen detonations varying in initial pressure and equivalence ratio. These detonations were performed during a measurement campaign in a newly-constructed linear detonation channel at the Air Force Research Laboratory at Edwards Air Force Base. Results from the CO and CO₂ speciation show a constant value trend of CO concentration and an upward trend of CO₂ concentration following the detonation wave.

Moving forward, there is significant future work associated with the data collected for this study: it should be noted that a total of 56 detonation experiments were performed in this measurement campaign, with multiple fuels, equivalence ratios, and initial pressures. Only a small subset has been discussed in this paper. Three vaporized liquid fuels were tested in this campaign including n-heptane, methanol, and isopropanol. Additionally, two sets of gaseous methane data sets were obtained for 1 atm and 0.5 atm initial fill pressures in the linear detonation channel. The analysis framework described in this paper will continue to be refined and subsequently applied to the remaining data sets. Lastly, to reduce the uncertainties in the interpretation of the data collected for CO₂, fundamental spectroscopy measurements behind reflected shock waves in the UTSA high-enthalpy shock tube [20] will be conducted while varying pressure and temperature to verify and refine the collisional line mixing model for CO₂.

Acknowledgments

This work is supported in part by the U.S. Air Force Office of Scientific Research (AFOSR), Grant No. FA9550-17-1-031, with Dr. Chiping Li as Program Officer, and the U.S. National Aeronautics and Space Administration (NASA), Grant. No. 80NSSC19M0194, and the U.S. National Science Foundation (NSF), Award No. 2135789. Additionally, this research was supported in part by the Air Force Research Laboratory Aerospace Systems Directorate, through the AFOSR Summer Faculty Fellowship Program®, Contract Numbers FA8750-15-3-6003, FA9550-15-0001 and FA9550-20-F-0005.

The authors thank Daniel D. Lee for valuable input during the development of the collisional line mixing model used to interpret CO₂ absorbance data collected in this study, and Anil P. Nair for helpful input on the implementation of bias-tee hardware and extended wavelength scanning techniques described in this paper.

References

[1] Hargus, W. A., Schumaker, S. A., and Paulson, E. J., "Air Force Research Laboratory Rotating Detonation Rocket Engine Development," 2018 Joint Propulsion Conference, American Institute of Aeronautics and Astronautics, Cincinnati, Ohio, 2018. https://doi.org/10.2514/6.2018-4876, URL https://arc.aiaa.org/doi/10.2514/6.2018-4876.

- [2] Zel'dovich, Y., "To the Question of Energy Use of Detonation Combustion," *Journal of Propulsion and Power*, Vol. 22, No. 3, 2006, pp. 588–592. https://doi.org/10.2514/1.22705
- [3] Nair, A. P., Lee, D. D., Pineda, D. I., Kriesel, J., Hargus, W. A., Bennewitz, J. W., Danczyk, S. A., and Spearrin, R. M., "MHz Laser Absorption Spectroscopy via Diplexed RF Modulation for Pressure, Temperature, and Species in Rotating Detonation Rocket Flows," *Applied Physics B*, Vol. 126, No. 8, 2020, p. 138. https://doi.org/10.1007/s00340-020-07483-8
- [4] Nair, A. P., Lee, D. D., Pineda, D. I., Kriesel, J., Hargus, W. A., Bennewitz, J. W., Bigler, B., Danczyk, S. A., and Spearrin, R. M., "Methane-oxygen rotating detonation exhaust thermodynamics with variable mixing, equivalence ratio, and mass flux," *Aerospace Science and Technology*, Vol. 113, 2021, p. 106683. https://doi.org/10.1016/j.ast.2021.106683. URL https://doi.org/10.1016/j.ast.2021.106683.
- [5] Bigler, B. R., Bennewitz, J. W., Danczyk, S. A., and Hargus, W. A., "Rotating detonation rocket engine operability under varied pressure drop injection," *Journal of Spacecraft and Rockets*, Vol. 58, No. 2, 2021, pp. 316–325. https://doi.org/10.2514/1.A34763.
- [6] Peng, H. Y., Liu, W. D., Liu, S. J., Zhang, H. L., and Huang, S. Y., "The competitive relationship between detonation and deflagration in the inner cylinder-variable continuous rotating detonation combustor," *Aerospace Science and Technology*, Vol. 107, 2020, p. 106263. https://doi.org/10.1016/j.ast.2020.106263. URL https://doi.org/10.1016/j.ast.2020.106263.
- [7] Hernandez-McCloskey, J., Pineda, D. I., Bennewitz, J. W., Bigler, B. R., Burr, J. R., Danczyk, S. A., Paulson, E. J., and Hargus, W. A., "Design and analysis of an additively manufactured rotating detonation rocket engine chamber for calorimetry and thermal management assessment," *AIAA SCITECH 2023 Forum*, American Institute of Aeronautics and Astronautics, Reston, Virginia, 2023, pp. 1–19. https://doi.org/10.2514/6.2023-0355, URL https://arc.aiaa.org/doi/10.2514/6.2023-0355.
- [8] Hanson, R. K., Spearrin, R. M., and Goldenstein, C. S., *Spectroscopy and Optical Diagnostics for Gases*, Springer International Publishing, Cham, Switzerland, 2016. https://doi.org/10.1007/978-3-319-23252-2.
- [9] Seber, G. A., and Wild, C., Nonlinear Regression, Wiley, 2003. https://doi.org/978-0-471-47135-6
- [10] Gordon, S., and Mcbride, B. J., "Computer Program for Calculation of Complex Chemical Equilibrium Compositions and Applications," NASA Reference Publication 1311, 1996.
- [11] Rothman, L. S., Gordon, I. E., Barber, R. J., Dothe, H., Gamache, R. R., Goldman, A., Perevalov, V. I., Tashkun, S. A., and Tennyson, J., "HITEMP, the high-temperature molecular spectroscopic database," *Journal of Quantitative Spectroscopy and Radiative Transfer*, Vol. 111, No. 15, 2010, pp. 2139–2150. https://doi.org/10.1016/j.jqsrt.2010.05.001, URL http://dx.doi.org/10.1016/j.jqsrt.2010.05.001.
- [12] Hartmann, J. M., Rosenmann, L., Perrin, M. Y., and Taine, J., "Accurate calculated tabulations of CO line broadening by H2O, N2, O2, and CO2 in the 200–3000-K temperature range," *Applied Optics*, Vol. 27, No. 15, 1988, p. 3063. https://doi.org/10.1364/ao.27.003063
- [13] Hartmann, J. M., Boulet, C., and Robert, D., Collisional Effects on Molecular Spectra, Elsevier, 2008. https://doi.org/10.1016/ B978-0-444-52017-3.X0001-5
- [14] Lee, D. D., Bendana, F. A., and Spearrin, R. M., "Exploiting line mixing effects for laser absorption spectroscopy at extreme combustion conditions," *11th U.S. National Combustion Meeting*, The Combustion Institute, Pasadena, CA, 2019.
- [15] Lee, D. D., Bendana, F. A., Nair, A. P., Pineda, D. I., and Spearrin, R. M., "Line mixing and broadening of carbon dioxide by argon in the v3 bandhead near 4.2 um at high temperatures and high pressures," *Journal of Quantitative Spectroscopy and Radiative Transfer*, Vol. 253, 2020, p. 107135. https://doi.org/10.1016/j.jqsrt.2020.107135, URL https://linkinghub.elsevier.com/retrieve/pii/S0022407319304042https://linkinghub.elsevier.com/retrieve/pii/S0022407320301151
- [16] Goldenstein, C. S., Spearrin, R. M., Jeffries, J. B., and Hanson, R. K., "Infrared laser-absorption sensing for combustion gases," *Progress in Energy and Combustion Science*, Vol. 60, 2017, pp. 132–176. https://doi.org/10.1016/j.pecs.2016.12.002
- [17] Nair, A. P., Minesi, N. Q., Jelloian, C., Kuenning, N. M., and Spearrin, R. M., "Extended tuning of distributed-feedback lasers in a bias-tee circuit via waveform optimization for MHz-rate absorption spectroscopy," *Measurement Science and Technology*, Vol. 33, No. 10, 2022, p. 105104. https://doi.org/10.1088/1361-6501/ac7b13. URL https://iopscience.iop.org/article/10.1088/1361-6501/ac7b13.
- [18] Bendana, F. A., Lee, D. D., Schumaker, S. A., Danczyk, S. A., and Spearrin, R. M., "Cross-band infrared laser absorption of carbon monoxide for thermometry and species sensing in high-pressure rocket flows," *Applied Physics B*, Vol. 125, No. 11, 2019, p. 204. https://doi.org/10.1007/s00340-019-7320-y.

- [19] Lee, D. D., Bendana, F. A., Nair, A. P., Danczyk, S. A., Hargus, W. A., and Spearrin, R. M., "Exploiting line-mixing effects for laser absorption spectroscopy at extreme combustion pressures," *Proceedings of the Combustion Institute*, Vol. 38, No. 1, 2021, pp. 1685–1693. https://doi.org/10.1016/j.proci.2020.08.037, URL https://doi.org/10.1016/j.proci.2020.08.037.
- [20] Steavenson, B. R., Alexander, A. T., Franklin, S. K., Bush, C. M., and Hernandez-McCloskey, J., "Design of the UTSA High-Enthalpy Shock Tube Facility," *AIAA SCITECH 2023 Forum*, American Institute of Aeronautics and Astronautics, Reston, Virginia, 2023, pp. 1–11. https://doi.org/10.2514/6.2023-0018, URL https://arc.aiaa.org/doi/10.2514/6.2023-0018.